Mitochondrial transfer alters cell fate by remodeling metabolic processes to regulate bone homeostasis

Yufeng Zhang (zyf@whu.edu.cn)
Wuhan University https://orcid.org/0000-0001-8702-5291
Wenjin Cai
Wuhan University
Jinglun Zhang
Wuhan University
Yiqian Yu
Wuhan University
Yueqi Ni
Wuhan University
Yan Wei
Wuhan University
Yihong Cheng
Wuhan University
Litian Han
Wuhan University
Leyi Xiao
Wuhan University
Xiaoxin Ma
Wuhan University
Hongjiang Wei
Wuhan University
Yaoting Ji
Wuhan University

Article

Keywords: Mesenchymal stem cells, Mitochondria, Macrophages, Intercellular Mitochondria transfer, Metabolism, Metabolic bone diseases

Posted Date: April 25th, 2022

DOI: https://doi.org/10.21203/rs.3.rs-1535811/v1

Abstract

Mitochondria are the powerhouse of eukaryotic cells, which regulate cell metabolism and differentiation. Recently, mitochondrial transfer between cells has been shown to direct recipient cell fate. However, it is unclear whether mitochondria can translocate to stem cells and whether this transfer alters stem cell fate. Here, we examined mesenchymal stem cell (MSC) regulation by macrophages in the bone marrow environment. We found that macrophages promote osteogenic differentiation of MSCs by delivering mitochondria to MSCs. However, under osteoporotic conditions, macrophages with altered phenotypes and metabolic statuses release oxidatively damaged mitochondria. The transfer of dysfunctional mitochondria to MSCs triggers a reactive oxygen species burst, which leads to metabolic remodeling. We showed that abnormal metabolism in MSCs is caused by the abnormal succinate accumulation, which is a key factor in abnormal osteogenic differentiation. These results reveal that mitochondrial transfer from macrophages to MSCs allows metabolic crosstalk to regulate bone homeostasis. This mechanism identifies a potential target for the treatment of osteoporosis.

Introduction

Coordinated activity of various cell types in the bone marrow is essential for maintaining homeostasis[1]. Bone homeostasis is mainly determined by the balance between bone resorption by osteoclasts and bone formation by osteoblasts and is closely related to the overall metabolism[2,3]. Compared to healthy people, patients with metabolism-related diseases caused by factors such as age and hormones have disrupted bone homeostasis and are at higher risk of osteoporosis and fragility-related fractures[3,4].

Osteoporosis is a systemic metabolic disease characterized by imbalanced bone homeostasis, low bone mass, and microstructural changes. Previous studies showed that immune cells, such as macrophages, are essential for maintaining bone homeostasis and are involved in the development of osteoporosis[5,6]. Macrophages are a heterogeneous population of cells that are converted to a pro-inflammatory (M1) or anti-inflammatory (M2) state in response to environmental stimuli. These cells regulate bone homeostasis by secreting related factors[5,7]. Macrophages promote osteogenic differentiation of mesenchymal stem cells (MSCs) through osteostatin (OS)-M and bone morphogenetic protein (BMP)-2 secretion[8,9]. Interleukin (IL)-6 and tumor necrosis factor (TNF)-α are secreted by proinflammatory M1-like macrophages and inhibit osteogenic functions[7,10,11]. Current research on signaling between macrophages and MSCs mainly focuses on how macrophages regulate MSC activity by paracrine signaling. However, in the complex bone marrow environment, whether there are additional direct communication modes needs further study.

Previous studies on intercellular communication focused on electrical coupling, paracrine signaling, and gap junction transmission. Recently, new communication modes that rely on organelle transfer between cells have received considerable attention[12]. Mitochondria are the energy source for eukaryotic cells and are crucial for regulating cell metabolism and differentiation. Thus, mitochondrial transfer is currently

receiving extensive attention[13–15]. Recipient cells can capture functional mitochondria released by donor cells into the extracellular space[13,16]. However, the circumstances under which mitochondrial transfer occurs and the underlying physiological implications require further investigation.

Previous studies confirmed that mitochondrial dysfunction is closely related to disease pathogenesis[17,18]. Since mitochondrial transfer may be involved in the pathogenesis of some diseases, interventions targeting the transfer process are currently under investigation[19,20]. Spees et al. demonstrated that mitochondria-depleted cells restore normal cellular viability by capturing healthy mitochondria from donor cells[21]. Other studies showed that when cells such as lung epithelium, cardiac muscle, and neurons are damaged, supplementing healthy mitochondria from MSCs can restore mitochondrial homeostasis and energy metabolism of the recipient cells[15,22]. However, the metabolic cascade in the target cells that are activated by mitochondrial transfer and the pathological processes intervened by mitochondrial transfer remain unclear. Further, how energy and MSC fate are regulated by other cells during mitochondrial transfer has not been well studied.

The bone marrow in which macrophages and MSCs are present is a freely dispersed environment. Therefore, it is necessary to investigate whether macrophages can transfer mitochondria to MSCs to regulate MSC fate. Here, we aimed to study macrophages that undergo mitochondria-specific energy stress to release oxidatively damaged mitochondria under osteoporotic conditions and the effect of dysfunctional mitochondria delivery on reactive oxygen species (ROS) production and osteogenic function of MSCs. Furthermore, our results suggest that circulating succinate induces elevated ROS levels and hypoxia inducible factor-1α (Hif-1α) activation to promote increased expression of pro-inflammatory genes, which in turn affects the osteogenic differentiation of MSCs. Collectively, cell-to-cell mitochondrial transfer in the bone marrow environment represents an underappreciated mechanism of cellular communication that has various regulatory effects on bone metabolism and provides new ideas for the prevention and treatment of osteoporosis.

Results

Macrophages deliver mitochondria to MSCs in the bone marrow

To verify mitochondrial transfer from macrophages to MSCs, we labeled MSCs with MitoTracker Green and co-cultured them with macrophages (labeled with MitoTracker Deep Red) for 0, 3, 6, and 24 h. Confocal microscopy and flow cytometry confirmed the presence of macrophage-derived mitochondria in MSCs (Fig. 1a, d, and e; Supplementary Video 1). Previous studies found that mitochondrial transfer relies on membrane carriers such as tunneling nanotubes (TNTs) and microvesicles (MVs) in most cases[23,24]. Moreover, free mitochondria or mitochondrial components can also be extruded or internalized into recipient cells. To investigate the mechanism of mitochondrial transfer and acceptance, we analyzed mitochondrial transfer from macrophages (labeled with MitoTracker Deep Red) to MSCs using a

transwell (TW) culture system (0.4 μm pore size) to isolate MSCs from macrophages. Mitochondrial transfer from macrophages to MSCs was partially inhibited in TW culture (Fig. 1b–e), indicating that free mitochondria or mitochondria-containing MVs can be internalized by MSCs. A transmission electron microscopy (TEM) analysis demonstrated that macrophages deliver mitochondria to MSCs in various ways, including free mitochondria, MVs, and TNTs. Further, these structures were internalized by MSCs (Supplementary Fig. 1a, b). MSC internalization was inhibited by dynasore, an endocytosis inhibitor that acts on dynamin-dependent clathrin activity but had no effect on MSC viability (Supplementary Fig. 1c-e).

To test whether intercellular mitochondrial transfer occurs *in vivo*, we extracted bone marrow-derived macrophages (BMDMs) for cell transplantation experiments. BMDMs were labeled with the mitochondrial marker protein Tom20 and used in subsequent experiments after flow cytometry (Supplementary Fig. 1f-h). BMDMs expressing Tom20-GFP were re-injected into irradiated mice via the tail vein. We analyzed the MSC phenotype using flow cytometry (Supplementary Fig. 1i) and found that green fluorescence appeared in MSCs, indicating that mitochondrial delivery from macrophages to MSCs occurs *in vivo* (Fig. 1f-i).

Mitochondrial function in macrophages is altered in osteoporosis

Macrophages are essential for regulating bone homeostasis[5,6]. Moreover, immune cell activation and function are closely related to cellular metabolism[25,26]. To investigate the metabolic profile of macrophages in osteoporosis, we used an ovariectomy (OVX) -operated mouse osteoporosis model. Using the flow cytometric analysis of F4/80 macrophages from sham and OVX mice, we assessed mitochondrial reactive oxygen species (mtROS) production by staining cells with 2,7-Dichlorodi - hydrofluorescein diacetate (DCFH-DA). The mtROS levels of BMDMs from OVX mice were higher than those in sham mice (Fig. 2a, b). We also analyzed the mitochondrial membrane potential (MMP) of the BMDMs. The flow cytometry of tetramethylrhodamine methyl ester (TMRM) showed that the MMP was elevated in BMDMs from OVX mice (Fig. 2c, d).

Next, we explored whether the expression of specific gene sets was induced under osteoporotic conditions to identify stage-specific metabolic profiles. We compared the macrophage transcriptomes in sham and OVX mice using RNA-seq. Principal component analysis (PCA) (Supplementary Fig. 2a) and hierarchical clustering (HC) ($p \leq 0.05$) (Fig. 2e) of the analyzed genes revealed profound transcriptional differences between macrophages between the sham and OVX groups. We found 1908 dysregulated genes with at least a 2-fold change (1220 upregulated and 688 downregulated) (Fig. 2f) in BMDMs treated with OVX compared with Sham-treated controls. We then performed Gene Ontology (GO) and Kyoto Encyclopedia of Genes and Genomes (KEGG) enrichment analyses based on the RNA-seq data (Fig. 2g; Supplementary Fig. 2b). The GO analysis revealed that the enrichments occurring in OVX rats mainly included the regulation of immune effector processes, responses to oxidative stress, mitochondrial organization, and mitochondrial ATP synthesis coupled with electron transport, carbohydrate transport, and glucose transmembrane transport (Fig. 2g). Metabolism-related pathways,

including HIF-1 and PI3K-Akt signaling, were enriched in osteoporosis (Supplementary Fig. 2b). Furthermore, compared to those of sham mice, BMDMs from OVX mice showed enrichment of specific mitochondrial processes, including Complex I, Complex III, reactive oxygen species, glutathione metabolism, carbohydrate metabolism, and the tricarboxylic acid (TCA) cycle (Fig. 2h).

Mitochondrial dysfunction in macrophages affects the osteogenic differentiation of MSCs

Macrophages are activated and polarized to M1-like (usually pro-inflammatory) or M2-like (usually anti-inflammatory) states in response to environmental factors[3,7]. We found that in the OVX osteoporosis mice, the percentage of $CD80^{+}F4/80^{+}$ M1 phenotype macrophages was significantly increased compared to that of sham mice (Fig. 3a). Furthermore, the percentage of $CD206^{+}F4/80^{+}$ M2 phenotype macrophages was significantly reduced by OVX, indicating a transition to the M1 phenotype (Fig. 3b). To further validate the phenotypic alterations in macrophages, we analyzed pro-inflammatory gene expression in BMDMs using qPCR. Inducible nitric oxide synthase (*Inos*), *IL-1β*, *TNF-α*, and *CD80* expression in OVX macrophages was higher than those in sham macrophages (Supplementary Fig. 3a-d). Furthermore, we found that endotoxin levels in the serum of OVX mice were higher than those in serum of sham mice (Supplementary Fig. 3e). These results demonstrate that macrophages are in a state of inflammatory activation when osteoporosis occurs.

We used a lipopolysaccharide (LPS)-induced bone loss model to explore whether higher endotoxin levels activate and polarize macrophages during osteoporosis. A micro-CT analysis confirmed substantial trabecular bone loss in LPS-treated mice compared to that in control mice (Fig. 3c-h). In LPS-treated mice, macrophages exhibited phenotypes similar to those in OVX mice, confirming that endotoxin levels affect macrophage polarization and metabolic status (Supplementary Fig. 3f-i).

Various genetic and chemical stresses trigger increased mitochondrial exchange in various cellular contexts. Inflammatory signaling receptor cells induced by LPS and TNF-α treatment are strong promoters of mitochondrial exchange[16,28]. The flow cytometric analysis showed that more mitochondria from OVX-derived macrophages were transferred to MSCs in the OVS group than those in the sham group (Fig. 3i, j). More mitochondrial transfer was also found by co-culturing RAW 264.7 cells (untreated or treated with LPS) and MSCs (Fig. 3k, l).

Next, we investigated whether mitochondria transferred from macrophages to MSCs regulate the osteogenic differentiation of MSCs. Indeed, MSCs that received normally functioning mitochondria showed an enhanced osteogenic phenotype compared with the MSC-alone group (Supplementary Fig. 4). In contrast, MSCs receiving dysfunctional mitochondria (OVX or LPS) showed impaired osteogenic capacity, such as decreased alkaline phosphatase (ALP) levels, decreased alizarin red-stained mineralized nodules, and decreased osteogenic gene expression (Supplementary Fig. 4). Then, we clarified how altered osteogenic function is influenced by mitochondrial transfer from macrophages. We extracted intact macrophage mitochondria and analyzed voltage-dependent anion channel (*Vdac*),

cytochrome c oxidase subunit IV isoform 1 (*COXIV*), and translocase of outer mitochondrial membrane 20 (*Tom20*) expression (Fig. 3m, n). Mineralization was induced in MSCs alone, MSCs cultured with normal mitochondria, and MSCs cultured with dysfunctional mitochondria (LPS treatment). These results confirm that dysfunctional mitochondria directly affected osteogenesis, showing lower ALP levels, fewer mineralized nodules, and decreased osteogenic gene expression (Fig. 3o, p).

Macrophages and derived mitochondria affect the metabolic status of MSCs

Energy metabolism in MSCs is closely related to osteoporosis occurrence and progression[3]. We investigated how mitochondrial transport from macrophages to MSCs affects the MSC metabolic state by measuring mtROS and MMP levels in MSCs. Mitochondria from LPS-treated macrophages led to increased ROS levels in MSCs, as measured by MitoSOX and DCFH-DA assays (Fig. 4a, c). Furthermore, the MMP of MSCs was significantly decreased (Fig. 4b, d).

We measured the steady-state ATP levels in MSCs to explore potential changes in bioenergetics (Fig. 4e). Increased ROS production and dysregulated ATP metabolism in MSCs demonstrated impaired mitochondrial function and reduced electron transport chain efficiency. Subsequently, we studied the impact of mitochondrial transfer on MSCs by metabolic profiling using the Seahorse platform. As previously described, we assessed basal respiration, proton leakage, and non-mitochondrial respiration[29]. Exposure to untreated macrophages enhanced respiration in MSCs. This transfer-enhanced respiration was abolished when macrophages were pretreated with LPS (Fig. 4f, g). Furthermore, we estimated the cellular glycolytic activity by assessing the extracellular acidification rate (ECAR) in MSCs. An increased ECAR level was observed after MSCs were incubated with LPS-treated macrophages (Fig. 4h, i). This metabolic shift to glycolysis was further supported by elevated glucose uptake (Fig. 4j) and increased cellular lactate levels (Fig. 4k). Finally, MSCs were incubated with mitochondria from untreated and LPS-treated macrophages. We observed that LPS-treated mitochondria promoted glycolysis (Fig. 5l, m) and reduced oxygen consumption (Fig. 5n, o).

Mitochondrial transfer causes abnormal succinate accumulation in MSCs

To investigate the molecular basis of metabolic reprogramming of MSCs by mitochondrial transfer, we analyzed the MSC transcriptome. We found that pro-inflammatory gene expression (including *IL-6* and *IL-1β*) were increased in the dysfunctional mitochondrial transfer group compared with that in the untreated macrophage and MSC groups (Fig. 5a). Interestingly, glycolytic genes were also upregulated (Fig. 5b), consistent with the increased ECAR (Fig. 4H and I). We then performed GO and KEGG enrichment analyses on the RNA-seq data. GO analysis showed that the MSCs in the dysfunctional mitochondrial transfer group showed changes in ROS metabolic process, ATP metabolic process, and mitochondrial organization (Fig. 5c). Furthermore, we found that the genes involved in the regulation of inflammatory

responses related to inflammatory activation and osteoclast differentiation in bone remodeling-related systems also changed (Fig. 5c).

Subsequently, we labeled MSCs with $^{13}C_6$-glucose and used mass spectrometry to trace the fate of glucose isotopes (Fig. 5e). We found that t the flux of glucose metabolism, was significantly altered in MSCs after dysfunctional mitochondrial transfer. Furthermore, in the dysfunctional mitochondrial transfer group, succinate, a TCA cycle intermediate, was elevated (Supplementary Fig. 5a). We observed succinate accumulation in MSCs in the osteoporosis-induced mice compared to that in mice in the sham and PBS groups (Fig. 5f, g). In BMDMs and serum of osteoporosis model mice, the succinate content also increased (Supplementary Fig. 5b-e). Interestingly, macrophages pretreated with succinate (5 mM) also influenced the succinate levels in MSCs (Fig. 5h). This abnormal succinate accumulation in MSCs of the dysfunctional mitochondrial transfer group may be related to the decreased activity of oxidases, such as succinate dehydrogenase (SDH) (Supplementary Fig. 5f).

Hif-1α plays a key role in glucose metabolism and bone resorption, and its activation is regulated by increased succinate levels[26,30,31]. Moreover, a sustained increase in succinate induces pro-inflammatory cytokine expression (such as IL-1β) via Hif-1α[26,32]. Accordingly, *Hif-1α* gene and protein expression in MSCs in the presence of LPS-treated macrophages were higher than those in the MSCs and untreated groups (Fig. 5i-k). MSCs in the dysfunctional mitochondrial transfer group were enriched in inflammatory and metabolism-related pathways such as the TNFα signaling pathway, NF-κB signaling pathway, oxidative phosphorylation, Hif-1α signaling pathway, and Toll-like signaling pathway. In addition, after pretreating macrophages with succinic acid, MSCs showed Hif-1α activation (Fig. 5l-m), upregulated glycolytic genes such as hexokinase 2 (*Hk2*) and solute carrier family 2 member 1 (*Slc2a1*), and upregulated pro-inflammatory genes such as *IL-1β* and *TNF-α* compared to those in the blank control group, (Supplementary Fig. 5g-p). These data suggest that succinate may directly regulate Hif-1α signaling and proinflammatory cytokine release, thereby affecting the osteogenic differentiation of MSCs.

Mitochondrial transfer maintains bone health in vivo

To examine the effect of dysfunctional mitochondria on skeletal health, we administered PBS and LPS-treated macrophage mitochondria [mito(LPS)] via the tail vein of 8-week-old mice twice a week for 4 weeks and analyzed their skeletal phenotype (Fig. 6a). Consistent with the histological data, a micro-CT analysis revealed lower trabecular volume and higher trabecular separation in the mito (LPS-treated) group than in the PBS group (Fig. 6b-h). We measured osteoclast bone resorption in mito(LPS) mice versus control mice and found that mito(LPS)-treated mice had more tartrate-resistant acid phosphatase (TRAP) + osteoclasts on the trabecular bone surface than in PBS-treated controls (Fig. 6i, g). Taken together, these results suggest that dysfunctional mitochondria disrupt skeletal homeostasis by reducing bone turnover.

Finally, we tested the effects of mitochondrial transfer on osteoporosis *in vivo*. We treated OVX mice by injecting mitochondria twice a week via the tail vein. von Kossa staining and micro-CT analysis of the

femur showed that mice treated with mitochondria displayed higher trabecular bone mass than the OVX group (Fig. 6k-q). Furthermore, the TRAP + osteoclasts were significantly reduced in OVX + mito-treated mice compared to those in OVX-treated mice (Fig. 6r, s).

Discussion

Our results demonstrated that macrophages in the bone marrow environment regulate the bioenergetic status and osteogenic differentiation of MSCs by transferring their mitochondria into MSCs. Under osteoporotic conditions, macrophages undergo mitochondrial dysfunction and transition into pro-inflammatory M1-like cells. This process leads to increased mitochondrial transfer from macrophages to MSCs. Moreover, the transfer of dysfunctional mitochondria to MSCs induces cellular damage and metabolic reprogramming. We also demonstrated that metabolic intermediates of the TCA cycle, such as succinate, increased in osteoporotic mice. Succinate regulates inflammation and is involved in multiple biological processes as a key signal. Succinate accumulation in MSCs promotes the increased expression of pro-inflammatory genes, including *IL-1β*, by inducing elevated ROS levels and Hif-1α activation, which in turn affects the osteogenic differentiation of MSCs.

Recently, the relationship between macrophage polarization and changes in the bone marrow environment have received extensive attention[3,33]. Under osteoporotic conditions, macrophages in the bone marrow environment exhibit altered mitochondrial functions, such as elevated ROS, increased mitochondrial membrane potential (MMP), and a shift to glycolysis. These results demonstrate that macrophages undergo inflammatory changes and mitochondrial dysfunction under osteoporotic conditions. Moreover, the development of various inflammatory states is regulated by endotoxin levels[3,34]. We observed elevated endotoxin levels in osteoporotic OVX mice, which further confirms that osteoporosis is a chronic inflammatory disease. To simulate impaired mitochondrial function *in vitro*, macrophages were treated with LPS. Changes in the mitochondrial function and the metabolic state of macrophages after LPS treatment were achieved by inhibiting complex II and III and remission state III respiration[26,35].

Mitochondria released from multiple cell types have been studied using *in vitro* and *in vivo* methods to validate cell-to-cell transfer[13,36]. However, the main focus of these studies is that damaged or cancer cells obtain mitochondria from donor cells (most likely MSCs) to rescue the metabolic and proliferative needs of the damaged cells[22,37]. There are far fewer reports on the role and underlying mechanism of mitochondrial transfer to MSCs. Only a few reports indicate that this phenomenon may be involved in the anti-apoptotic and pro-differentiation functions of activated stem cells[38,39]. Levoux et al. demonstrated that platelets enhance the therapeutic effect of MSCs on wound healing, whereas platelets with dysfunctional mitochondrial affect the therapeutic capacity of MSCs[13]. The donor cell type and functional status may have different effects on recipient cells after mitochondrial transfer[37,40]. A similar phenomenon was observed in our study; when infused with dysfunctional mitochondria (LPS-treated),

mice developed osteoporosis-like symptoms, whereas infusing normal mitochondria ameliorated the bone loss symptoms after OVX surgery.

Substantial evidence suggests that cell-to-cell mitochondrial transfer occurs more frequently in organisms than previously thought[13,22,38]. Mitochondrial transfer between cells regulates cellular function and the energy metabolism state of recipient cells through mitochondrial integration[13,23]. In our experiments, we observed that when dysfunctional mitochondria were transferred to MSCs, mitochondrial abnormalities such as increased ROS and decreased MMP were induced. Simultaneously, we found that oxygen consumption in MSCs decreased and glycolysis increased during this process. This evidence suggests that dysfunctional mitochondria change the metabolic state of MSCs, which in turn leads to osteogenic differentiation disorders.

Subsequently, we verified how mitochondria from M1-like macrophages affect TCA cycle metabolism in recipient MSCs. Several intermediates of the TCA cycle, including succinic acid, were upregulated. Succinate is an important metabolite in host and microbial processes and is involved in various pathophysiological processes *in vivo*[41,42]. Circulating succinate levels are elevated in metabolic and inflammation-related diseases, including ischemic heart disease[43], obesity[44], and type 2 diabetes[4,44]. Guo et al. concluded that hyperglycemia induces succinate accumulation in bone marrow stromal cells, which in turn stimulates osteoclastogenesis[4]. The development of metabolic disorders in skeletal disorders is controlled by succinate, but the mechanism remains unknown. Notably, abnormal ROS elevation during ischemia-reperfusion injury is controlled by succinate accumulation, and ROS levels affect the severity of tissue damage[45].

In addition to inducing ROS production, high succinate levels directly inhibit the prolyl hydroxylase domain (PHD) to regulate Hif-1α stability. Succinate accumulation induces the transcription of many inflammatory genes, including those encoding IL-1β, through Hif-1α, which plays an important role in glycolytic reprogramming[26]. However, local transplantation of human MSC-EVs also induces Hif-1α expression, and Hif-1α-mediated *Vegfa* expression is a key regulator that promotes angiogenesis and accelerates fracture healing [46]. This mechanism is consistent with the results of our OVX recovery experiments. We observed that Hif-1α increased when macrophages and MSCs were co-cultured, but MSCs showed enhanced osteogenic differentiation ability. We hypothesized that MSC differentiation ability may be affected by succinate-regulated inflammatory genes. Succinate levels did not increase in MSCs after normal mitochondrial transfer. Therefore, inflammatory activation is regulated by intracellular succinate levels in MSCs after mitochondrial transfer and is critical for MSC metabolism and differentiation.

This study focused on mitochondrial delivery from macrophages to MSCs for two reasons. 1) Our experiments verified whether the bone marrow environment in osteoporosis is in an inflammatory state and macrophages respond faster and more directly. 2) MSCs, a stem cell population that provides osteoblasts in the bone marrow environment, have high research and application potential to study the

effects of other factors on their cell status. In future experiments, we will examine mitochondrial transfer from MSCs to macrophages and their regulation in more detail.

Our findings reveal a new pattern of cellular crosstalk in the bone marrow environment, with macrophages regulating bone metabolism crosstalk by transferring their mitochondria into MSCs. This study suggests that mitochondrial transfer may be a novel way to regulate homeostasis by enabling immune cells to regulate their local tissue environment. Targeting mitochondrial transfer to prevent bone loss provides a new approach to the treatment and prevention of osteoporosis and proposes additional strategy to improve metabolism-related diseases.

Methods

Mice

Female C57BL/6 mice were obtained from the Animal Center of Wuhan University. All experimental procedures were approved by Wuhan University and were performed according to laboratory animal care and use guidelines.

For the LPS (Solarbio) induced calcium osteolysis mouse model, female C57BL/6 mice (8 weeks old) were randomly assigned to three groups: PBS group (n = 10), LPS group (5 mg/kg LPS, n = 10), and mito(LPS) group (100 μg LPS-Mito, n = 10). LPS (5 mg/kg) was injected intraperitoneally once per week for 3 weeks. Mito(LPS) (100 μg dissolved in 100 μL PBS) was injected through the tail vein twice weekly for 3 weeks.

Ovariectomy was performed at 8 weeks of age, as described previously [47]. For the postmenopausal osteoporosis model, the mice were divided into three groups: sham mice (sham, n = 10), OVX mice (OVX, n = 12), and Mito mice (OVX + Mito, n = 10). Raw Mito (100 μg dissolved in 100 μL PBS) was injected through the tail vein twice a week starting 1 week after surgery for 6 weeks.

Blood samples were centrifuged at 1,000×g for 15 min to harvest the serum, which was stored at −80°C for later use. Femurs were also collected.

For the BMDM transplantation experiment, mice received 8 Gy irradiation from a cesium-137 irradiator. Mitochondria from BMDMs overexpressing TOM20-GFP were intravenously injected into irradiated mice. At 24 hours after irradiation, $1x10^6$ BMDM TOM20-GFP cells were transplanted via a tail vein injection. The mice were analyzed 24 h after transplantation.

BMDM and MSC isolation and culture

BMDMs were extracted from the leg bones, differentiated in DMEM (Gibco) containing 10% fetal bovine serum (FBS, Gibco), 1% penicillin streptomycin (Gibco), and macrophage colony-stimulating factor (M-CSF) (50 ng/mL) (Proteintech) for 72 h. Unless otherwise stated, $5.0x10^5$ BMDM/mL were used for *in vitro* experiments.

MSCs were originally isolated from the tibias and femurs of mice. The bone marrow was washed with α-Dulbecco's medium (α-MEM; Gibco). The adherent cell population was left behind in standard α-MEM containing 20% FBS. The cells were further purified by passage, and cells from passage 3 were used for subsequent experiments. The cells were grown in a humidified 5% CO_2 atmosphere at 37°C.

Assessment of mitochondrial transfer from macrophages to MSCs

To evaluate mitochondrial transfer, MSCs and macrophages were labeled with MitoTracker Green (100 nM, Invitrogen) and MitoTracker Deep Red (100 nM, Invitrogen), respectively. Mitochondrial transfer was analyzed using co-cultures and Transwell plates containing 0.4 μm pore polycarbonate membranes (Millipore). An LSR Fortessa X20 flow cytometer (BD Biosciences) or an LSM800 confocal microscope (Zeiss) was used to detect macrophage-derived mitochondria in MSCs. Mitochondrial transfer and MSC viability were analyzed by flow cytometry and cell counting kit-8 (CCK8) viability assays after treatment with 50 μM dynasore (a dynamin-dependent clathrin-mediated endocytosis inhibitor) (MedChemExpress) for 24 h.

Flow cytometry

As previously described [48], MSCs exhibited the following phenotypes: $CD29^+$ (BioLegend; 1:200), stem cell antigen 1 $(Sca\text{-}1)^+$ (Invitrogen; 1:200), $CD73^+$ (BioLegend; 1:200), $CD44^+$ (BioLegend; 1:100), CD34- (BioLegend; 1:100), and $CD45^-$ (BioLegend; 1:200). BMDMs were incubated with F4/80-APC-Cy7 (Biolegend; 1:400), CD206-FITC (BioLegend; 1:200), and CD80-PE-Cy5 (BioLegend; 1:200) antibodies at 4°C for 30 min. Then, the ratios of CD206/F4/80 and CD80/F4/80 cells were analyzed. Labeled cells were collected and analyzed using a FACScan flow cytometer (Becton Dickinson). Data were analyzed using FlowJo software.

Osteogenic differentiation assay

For osteoblast differentiation, MSCs were cultured in DMEM containing 10% FBS, 100 nM dexamethasone (Sigma), 50 μg/mL ascorbic acid (Sigma), and 5 mM β-glycerophosphate (Sigma). After culturing for 7 days, cells were stained using a BCIP/NBT alkaline phosphatase color reagent kit (Beyotime) to evaluate alkaline phosphatase content. After incubation for 14 days, cells were stained with 0.2% alizarin red (pH 4.2, Sigma-Aldrich) to evaluate the degree of mineralization.

Transmission electron microscopy

MSCs were seeded at a density of 16×10^4 cells/mL in 12-well plates and co-cultured with RAW 264.7 cells (mouse mononuclear macrophage leukemia cells) for 24 hours. The cells were fixed with 3% glutaraldehyde for 5 min at room temperature, washed three times with PBS, and post-fixed with 1% osmium tetroxide. The fixed cells were dehydrated in an ascending ethanol series (70%, 90%, and 100%) and infiltrated and embedded in epoxy resin [24]. After the samples were sliced (70 nm) with a diamond knife, the sections were picked using a copper grid (100 mesh). After staining with uranyl acetate and

lead citrate, the samples were observed using a JEM-1400 transmission electron microscope (JEOL) at an acceleration voltage of 120 kV.

Mitochondrial isolation and quantification

The method for isolating mitochondria from the cells was optimized according to the manufacturer's protocol (Solarbio). Conditioned cells were washed with PBS and collected. Ice-cold lysis buffer was added to resuspend the cells, which were lysed with a tissue homogenizer in an ice bath at 0°C. Mitochondria were obtained after gradient centrifugation. The mitochondrial protein concentration was determined using the BCA protein quantification Kit.

Real-time PCR assays

Total RNA from BMDM and MSC were isolated using TRIzol reagent (Takara). cDNA was prepared by reverse transcription of 1 μg total RNA using HiScript II Q RT SuperMix (Vazyme). Amplification reactions were performed using ChamQ SYBR qPCR master mix (Vazyme) and random primers. The $2^{-\Delta\Delta Ct}$ method was used to quantify relative expression, which was normalized to β-actin levels.

Western blot

Total intracellular protein was extracted using pre-cooled RIPA lysis buffer. Protein concentrations were detected using a BCA protein assay kit (Beyotime). Samples with equal protein concentrations were separated by 10% SDS-PAGE. The proteins were transferred to PVDF membranes (Roche). The membranes were blocked with skim milk for 1 h at room temperature and incubated with primary antibody overnight at 4°C. Membranes were incubated with appropriate HRP-conjugated secondary antibody (ABclonal; 1:1,0000) for 1 h at room temperature. Signals were detected using enhanced chemiluminescence reagent (ECL, Advansta). The following primary antibodies were used for Western blot analysis at the indicated dilutions: anti-Vdac (ABclonal, 1:1000), anti-COXIV (ABclonal, 1:1000), anti-Tom20 (ABclonal, 1:1000), anti-Hif-1α (ABclonal, 1:1000), and anti-β-actin (ABclonal, 1:1000).

Endotoxin measurements

Serum, BMDM, and MSC endotoxin levels were determined using an LAL Chromogenic Endotoxin Quantitation Kit (Pierce). The serum was diluted 1:50 under pyrogen-free conditions and inactivated at 70°C for 15 min. Limulus reagent was added and incubated at 37°C for 8 min. The cells were incubated for 6 min after adding developer. After adding the stop reaction solution, 100 μL sample was pipetted into a pyrogen-free 96-well plate and use a microplate reader (Molecular Devices) to measure the absorbance at 405 nm.

Confocal and FACS determination of ROS

Intracellular mitochondrial ROS production was measured using MitoSOX probe (Life Technologies). The cells were mixed with 3 μM MitoSOX Red (Invitrogen) and 100 nM MitoTracker Green in PBS and incubated at 37°C for 30 min. The cells were assayed for mitochondrial ROS using confocal microscopy.

Additionally, cells were mixed with 10 μM DCFH-DA (Beyotime) and incubated at 37°C for 20 min and analyzed using a flow cytometer (Becton Dickinson). Data were analyzed using FlowJo software.

Confocal and FACS determination of tetramethylrhodamine methyl ester

The membrane potential of intracellular mitochondria was measured using TMRM (Invitrogen). Cells were incubated in TMRM (100 nM) for 20 min at 37°C. Cells were imaged using a confocal microscope (Zeiss, Jena, Germany). For flow cytometry assays, the cells were trypsinized into single cell suspensions and resuspended in PBS. The TMRM intensity in different groups was measured using a flow cytometer (Becton Dickinson) and the data were analyzed using FlowJo software.

Metabolic analysis

Energy metabolism analysis was performed using an XF24 extracellular flux analyzer (Seahorse Bioscience). Briefly, cells were seeded into XF24 cell culture plates (Seahorse Bioscience) at 8×10^4 cells per well after treatment as described earlier. The plate containing the syringe ports and probes and the utility plate containing calibrator solution (1 mL/well) were placed together in a CO_2-free incubator at 37°C overnight. The next day, the original medium was replaced with XF assay buffer (XF basic medium supplemented with 25 mM glucose, 1 mM pyruvate, 2 mM L-glutamine, and adjusted to pH 7.4). The cell culture plate was placed in a CO_2-free incubator for at least 0.5 h. Inhibitors [1 μM oligomycin, 1 μM carbonyl cyanide-4-(trifluoromethoxy)phenylhydrazone (FCCP), 1 μM rotenone, 10 mM glucose, and 50 mM 2-Deoxy-D-glucose (2DG]) were added to the port of the syringe plate. The plate was run using the utility plate for calibration. After completion, the utility plate was replaced with a cell culture plate for the run. Data were analyzed using Seahorse Wave software 2.6.1. The data were normalized using the protein content.

RNA-seq and data analysis

Total RNA was extracted from BMDM and MSC cells using the TRIzol reagent (Takara). Purified poly(A) mRNA was isolated from 1 mg total RNA using a Poly(A) mRNA Magnetic Isolation Module (Thermo Scientific). Then, RNA-seq libraries were prepared using NEBNext Super Directional RNA Library Preparation Kits (New England Biolabs). Sequencing was performed on an Illumina NovaSeq 6000 platform with 150-bp paired-end reads. Raw sequencing data were processed by Trim_Galore (v.0.6.7) for removing adapters and low-quality base pairs. The reads were mapped to the mouse reference genome (GRCm38) using HISAT2 software (v.2.1.0). The number of reads mapped to each Ensembl gene was counted using featureCounts(v.2.0.1). Sequence count data normalization and differential expression analysis was performed using R/Bioconductor package DESeq2 (v1.32.0).

Micro-CT analysis and bone histomorphometry

Mouse femurs were fixed with 4% paraformaldehyde for 24 h at 4°C and scanned using a high-resolution micro-computed tomography scanner (SkyScan). The scanner was set at 80 kV, 100 mA, and 6 mm/pixel

resolution. The region of interest (ROI) was analyzed from 0.1 mm below the growth plate to 5% of the femur length. A three-dimensional analysis of the following morphological parameters was performed using CTAn (Brucker): bone volume (BV), trabecular bone volume per tissue volume (Tb.BV/TV), trabecular number (Tb.N), trabecular thickness (Tb.Th), and trabecular separation (Tb.Sp). For histomorphometry, femurs were decalcified with 10% EDTA and paraffin-embedded; 5-μm sections were prepared using a microtome (Leica) and stained with von Kossa and TRAP (Sigma). Image analysis was performed using bone histomorphological parameters 69 and ImageJ.

$^{13}C_6$-Glucose LC-MS Metabolomics

MSCs were seeded into 6-well plates at a density of 40×10^4/well and were divided into control, RAW-Transwell, and RAW + LPS-Transwell groups. The cells were cultured in DMEM for 24 h. The media was then replaced with homogeneously labeled DMEM containing 25 mM $^{13}C_6$-glucose (Sigma) and incubated for 4 h. The cells were gently washed three times with ice-cold PBS. Then, 1 mL pre-chilled 80% methanol was added to each well, and the cells were lysed at -80°C for 2 h. The lysate was collected and centrifuged at 14,000 × g for 20 min at 4°C. The protein concentrations in the extracts were determined using a BCA protein quantification Kit. The supernatant was dried using a Speedvac instrument. Metabolite measurements were performed using the Tsinghua University Metabolomics platform. ^{13}C enrichment in glucose was determined using LC-MS [26]. The expected retention times and accurate masses were measured using TraceFinder 4.1 (Thermo Scientific) and target metabolites were quantified using the area under the curve. Cell numbers and sample protein concentrations were used for normalization. The relative metabolite levels were calculated by summing the values for all isotopologs of a given metabolite. The ^{13}C carbon relative to the total carbon was calculated for each metabolite.

Colorimetric determination of succinate

We used a succinate (succinic acid) assay kit (BioVision Inc.) according to the manufacturer's manual. Succinate levels were detected in serum, BMDM and MSC samples. 50 μl of samples and standards were sequentially added to 96-well plates, incubated at 37°C for 30 min, and use a microplate reader (Molecular Devices) to measure the absorbance at 450 nm.

Statistical analysis

Statistical analysis was performed using GraphPad Prism 8.0 (GraphPad Software). The data are presented as the mean ± SD, showing continuous normal distribution. Two sample groups were analyzed using two-tailed Student's t-test. Multiple groups were analyzed using one-way or two-way ANOVA. Differences were considered statistically significant at $p < 0.05$. *$p < 0.05$, **$p < 0.01$, and ***$p < 0.001$.

Declarations

Acknowledgements

This work was supported by National Key R&D Program of China (Grant No. 2021YFC2400405), the National Natural Science Foundation of China (Grant No. 82172493) and the National Natural Science Foundation of China for Distinguished Young Scholars (Grant No. 82025011).

Footnotes

Contributed by

Author contributions

Wenjin Cai, Yaoting Ji and Yufeng Zhang conceived this research. Wenjin Cai, Jinglun Zhang conducted most experiments with the help of Yueqi Ni, Yan Wei and Leyi Xiao. Wenjin Cai, Yiqian Yu and Litian Han performed bioinformatic analysis. Wenjin Cai and Jinglun Zhang wrote this paper. Wenjin Cai and Yihong Cheng analyzed the data. Wenjin Cai and Yaoting ji revised the document. All authors read and approved the final manuscript.

Data Availability

The data that support the findings of this study are available from the corresponding author upon request

Competing Interests

The authors declare no competing interests.

References

1. van Gastel, N. & Carmeliet, G. Metabolic regulation of skeletal cell fate and function in physiology and disease. Nature Metabolism **3**, 11–20 (2021).
2. Lee, W.C., Ji, X., Nissim, I. & Long, F. Malic Enzyme Couples Mitochondria with Aerobic Glycolysis in Osteoblasts. Cell reports **32**, 108108 (2020).
3. Li, C.J., *et al.* Senescent immune cells release grancalcin to promote skeletal aging. Cell metabolism **34**, 184–185 (2022).
4. Guo, Y., Xie, C. & Li, X. Succinate and its G-protein-coupled receptor stimulates osteoclastogenesis. Nature Communications **8**, 15621 (2017).
5. Gao, B., *et al.* Macrophage-lineage TRAP + cells recruit periosteum-derived cells for periosteal osteogenesis and regeneration. The Journal of clinical investigation **129**, 2578–2594 (2019).
6. Michalski, M.N., Koh, A.J., Weidner, S., Roca, H. & McCauley, L.K. Modulation of Osteoblastic Cell Efferocytosis by Bone Marrow Macrophages. Journal of cellular biochemistry **117**, 2697–2706 (2016).
7. Kim, P.G. & Niroula, A. Dnmt3a-mutated clonal hematopoiesis promotes osteoporosis. Journal of Experimental Medicine **218**(2021).

8. Guihard, P., *et al.* Induction of osteogenesis in mesenchymal stem cells by activated monocytes/macrophages depends on oncostatin M signaling. Stem cells (Dayton, Ohio) **30**, 762–772 (2012).
9. Zhang, Y., *et al.* Macrophage type modulates osteogenic differentiation of adipose tissue MSCs. Cell and tissue research **369**, 273–286 (2017).
10. Harmer, D., Falank, C. & Reagan, M.R. Interleukin-6 Interweaves the Bone Marrow Microenvironment, Bone Loss, and Multiple Myeloma. Frontiers in endocrinology **9**, 788 (2018).
11. Sun, W., Meednu, N., Rosenberg, A., Rangel-Moreno, J. & Wang, V. B cells inhibit bone formation in rheumatoid arthritis by suppressing osteoblast differentiation. **9**, 5127 (2018).
12. Rogers, R.S. & Bhattacharya, J. When cells become organelle donors. Physiology (Bethesda, Md.) **28**, 414–422 (2013).
13. Levoux, J., *et al.* Platelets Facilitate the Wound-Healing Capability of Mesenchymal Stem Cells by Mitochondrial Transfer and Metabolic Reprogramming. Cell metabolism **33**, 283–299.e289 (2021).
14. Brestoff, J.R., *et al.* Intercellular Mitochondria Transfer to Macrophages Regulates White Adipose Tissue Homeostasis and Is Impaired in Obesity. Cell metabolism **33**, 270–282.e278 (2021).
15. Liu, D., *et al.* Intercellular mitochondrial transfer as a means of tissue revitalization. Signal Transduction and Targeted Therapy **6**, 65 (2021).
16. Islam, M.N., *et al.* Mitochondrial transfer from bone-marrow-derived stromal cells to pulmonary alveoli protects against acute lung injury. Nature medicine **18**, 759–765 (2012).
17. Gorman, G.S., *et al.* Mitochondrial diseases. Nature reviews. Disease primers **2**, 16080 (2016).
18. Sanderson, T.H., Reynolds, C.A., Kumar, R., Przyklenk, K. & Hüttemann, M. Molecular mechanisms of ischemia-reperfusion injury in brain: pivotal role of the mitochondrial membrane potential in reactive oxygen species generation. Molecular neurobiology **47**, 9–23 (2013).
19. Mittelbrunn, M. & Sánchez-Madrid, F. Intercellular communication: diverse structures for exchange of genetic information. Nature reviews. Molecular cell biology **13**, 328–335 (2012).
20. Valenti, D. & Vacca, R.A. Mitochondria Can Cross Cell Boundaries: An Overview of the Biological Relevance, Pathophysiological Implications and Therapeutic Perspectives of Intercellular Mitochondrial Transfer. International Journal of Molecular Sciences **22**(2021).
21. Spees, J.L., Olson, S.D., Whitney, M.J. & Prockop, D.J. Mitochondrial transfer between cells can rescue aerobic respiration. Proceedings of the National Academy of Sciences of the United States of America **103**, 1283–1288 (2006).
22. Huang, T. & Zhang, T. Iron oxide nanoparticles augment the intercellular mitochondrial transfer-mediated therapy. Science Advances **7**, eabj0534 (2021).
23. Saha, T. & Dash, C. Intercellular nanotubes mediate mitochondrial trafficking between cancer and immune cells. Nature Nanotechnology **17**, 98–106 (2022).
24. Boudreau, L.H., *et al.* Platelets release mitochondria serving as substrate for bactericidal group IIA-secreted phospholipase A2 to promote inflammation. Blood **124**, 2173–2183 (2014).

25. Willenborg, S., *et al.* Mitochondrial metabolism coordinates stage-specific repair processes in macrophages during wound healing. Cell metabolism **33**, 2398–2414.e2399 (2021).
26. Mills, E.L., *et al.* Succinate Dehydrogenase Supports Metabolic Repurposing of Mitochondria to Drive Inflammatory Macrophages. Cell **167**, 457–470.e413 (2016).
27. Murphy, M.P. How mitochondria produce reactive oxygen species. The Biochemical journal **417**, 1–13 (2009).
28. Ahmad, T., *et al.* Miro1 regulates intercellular mitochondrial transport & enhances mesenchymal stem cell rescue efficacy. The EMBO journal **33**, 994–1010 (2014).
29. Ryall, J.G. Simultaneous Measurement of Mitochondrial and Glycolytic Activity in Quiescent Muscle Stem Cells. Methods in molecular biology (Clifton, N.J.) **1556**, 245–253 (2017).
30. Görlach, A. & Bonello, S. The cross-talk between NF-kappaB and HIF-1: further evidence for a significant liaison. The Biochemical journal **412**, e17-19 (2008).
31. Indo, Y., *et al.* Metabolic regulation of osteoclast differentiation and function. Journal of bone and mineral research: the official journal of the American Society for Bone and Mineral Research **28**, 2392–2399 (2013).
32. Tannahill, G.M., *et al.* Succinate is an inflammatory signal that induces IL-1β through HIF-1α. Nature **496**, 238–242 (2013).
33. Ambrosi, T.H., *et al.* Adipocyte Accumulation in the Bone Marrow during Obesity and Aging Impairs Stem Cell-Based Hematopoietic and Bone Regeneration. Cell stem cell **20**, 771–784.e776 (2017).
34. Fabbiano, S., *et al.* Functional Gut Microbiota Remodeling Contributes to the Caloric Restriction-Induced Metabolic Improvements. Cell metabolism **28**, 907–921.e907 (2018).
35. Kato, M. Site of action of lipid A on mitochondria. Journal of bacteriology **112**, 268–275 (1972).
36. Pollara, J., Edwards, R.W., Lin, L., Bendersky, V.A. & Brennan, T.V. Circulating mitochondria in deceased organ donors are associated with immune activation and early allograft dysfunction. JCI insight **3**(2018).
37. Rodriguez, A.M., Nakhle, J., Griessinger, E. & Vignais, M.L. Intercellular mitochondria trafficking highlighting the dual role of mesenchymal stem cells as both sensors and rescuers of tissue injury. Cell cycle (Georgetown, Tex.) **17**, 712–721 (2018).
38. Koyanagi, M., Brandes, R.P., Haendeler, J., Zeiher, A.M. & Dimmeler, S. Cell-to-cell connection of endothelial progenitor cells with cardiac myocytes by nanotubes: a novel mechanism for cell fate changes? Circulation research **96**, 1039–1041 (2005).
39. Mahrouf-Yorgov, M., *et al.* Mesenchymal stem cells sense mitochondria released from damaged cells as danger signals to activate their rescue properties. Cell death and differentiation **24**, 1224–1238 (2017).
40. Nakhle, J., Rodriguez, A.M. & Vignais, M.L. Multifaceted Roles of Mitochondrial Components and Metabolites in Metabolic Diseases and Cancer. International journal of molecular sciences **21**(2020).

41. Fernández-Veledo, S. & Vendrell, J. Gut microbiota-derived succinate: Friend or foe in human metabolic diseases? Reviews in endocrine & metabolic disorders **20**, 439–447 (2019).
42. Jiang, S. & Yan, W. Succinate in the cancer-immune cycle. Cancer letters **390**, 45–47 (2017).
43. Aguiar, C.J., *et al.* Succinate causes pathological cardiomyocyte hypertrophy through GPR91 activation. Cell communication and signaling: CCS **12**, 78 (2014).
44. Serena, C., *et al.* Elevated circulating levels of succinate in human obesity are linked to specific gut microbiota. ISME Journal **12**, 1642–1657 (2018).
45. Kula-Alwar, D., Prag, H.A. & Krieg, T. Targeting Succinate Metabolism in Ischemia/Reperfusion Injury. Circulation **140**, 1968–1970 (2019).
46. Gao, J., Qin, A., Liu, D. & Ruan, R. Endoplasmic reticulum mediates mitochondrial transfer within the osteocyte dendritic network. Science Advances **5**, eaaw7215 (2019).
47. Hu, Y., *et al.* Human umbilical cord mesenchymal stromal cells-derived extracellular vesicles exert potent bone protective effects by CLEC11A-mediated regulation of bone metabolism. Theranostics **10**, 2293–2308 (2020).
48. Houlihan, D.D., *et al.* Isolation of mouse mesenchymal stem cells on the basis of expression of Sca-1 and PDGFR-α. Nature protocols **7**, 2103–2111 (2012).

Figures

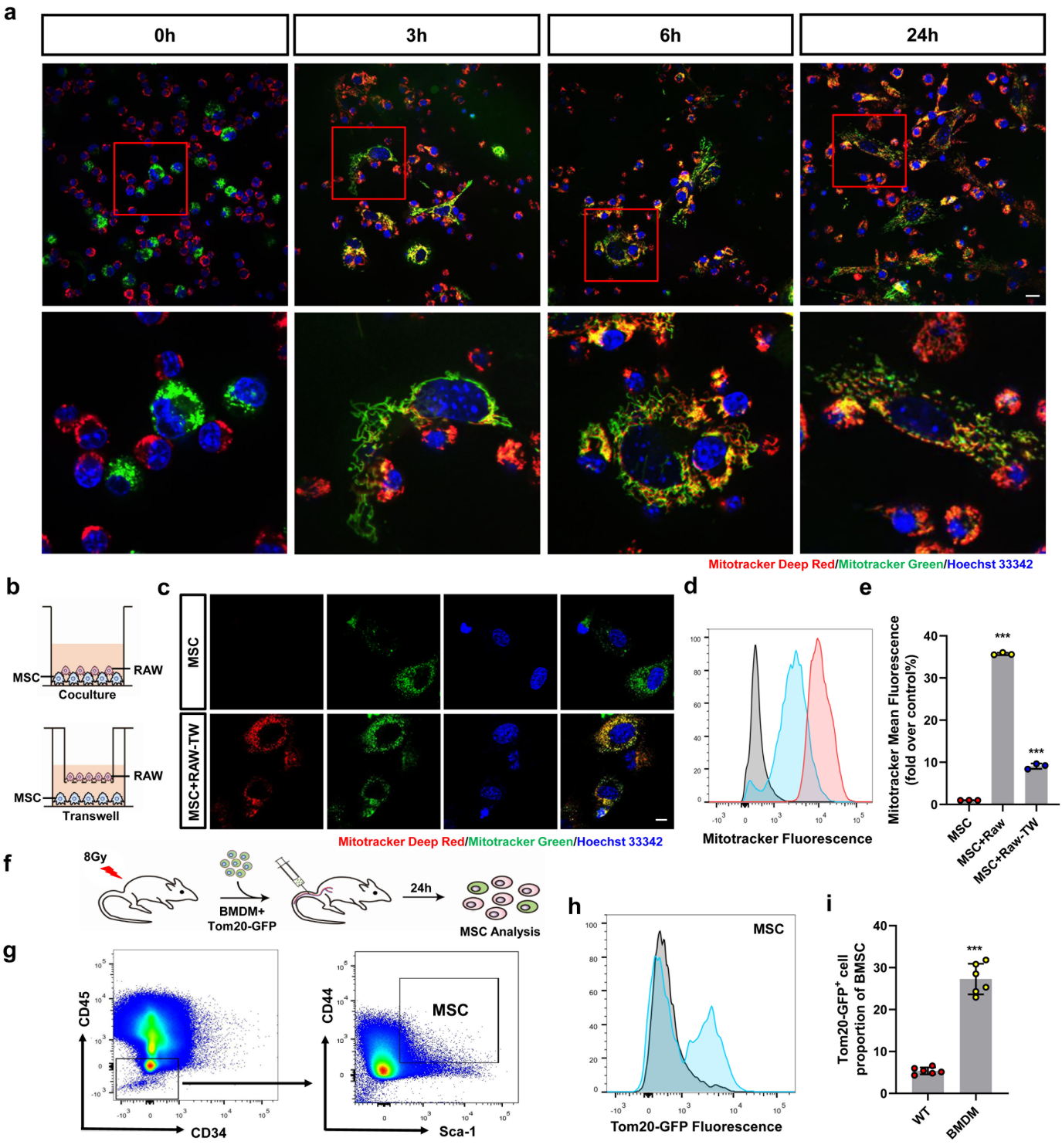

Figure 1

Macrophages deliver mitochondria to MSCs in the bone marrow.

(a) Representative confocal microscopy pictures of macrophages incubated with MSCs for 0, 3, 6, and 24 hours, MSCs were previously labeled with Mitotracker Green (green signal), and macrophages were labeled with Mitotracker Deep Red (red signal), Nuclei were labeled with Hoechst 33342 (blue signal) (n =

3). Scale bar, 10 μm. (b–e) The co-culture system and the TW culture system determine the mitochondrial transfer form (b). Comparison by confocal microscopy (c) and flow cytometry (d). Quantification of mitochondrial internalization was performed by flow cytometry (e). Grey line, untreated MSCs. Blue line, MSCs exposed to untreated macrophages. Red line, MSCs exposed to macrophages treated with the TW system (n = 3). Scale bar, 5 μm. (f-i) Schematic representation of mitochondrial transfer assessment in vivo (f). Flow cytometry quantified the transfer of mitochondria from Tom20-GFP-labeled BMDMs to MSCs (g) and quantified the mean fluorescence intensity of GFP (h, i) (n = 6). *P < 0.05, **P < 0.01, ***P < 0.001.

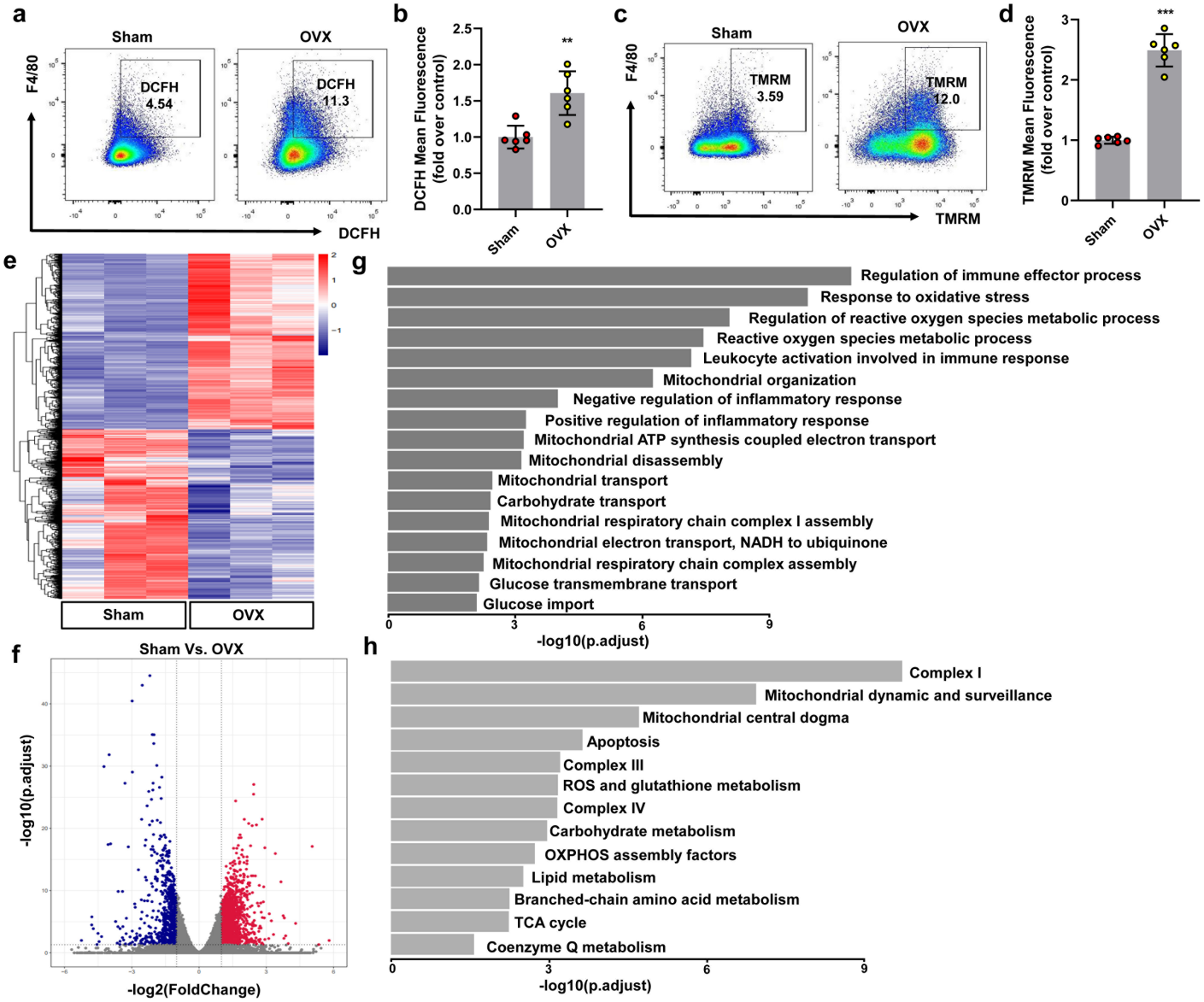

Figure 2

Mitochondrial function of macrophages is altered in osteoporosis.

(a, b) Macrophages were co-treated with DCFH-DA and F4/80 for 30 min, by flow cytometry to quantify ROS and mean fluorescence intensity as a measure of cellular reactive oxygen species production (n = 6). (c, d) Macrophages were co-treated with TMRM (20 nM) and F4/80 for 30 min and then analyzed by flow cytometry to quantify membrane potential (n = 6). (e–h) RNA-seq analysis in Sham or OVX-treated BMDMs (n = 3). (e) Genes shown by HC. (f) Volcano plot of all identified genes. (g) GO analysis. (h) GO analysis of genes encoding proteins with mitochondrial localization (based on MitoCarta 3.0 dataset). *P < 0.05, **P < 0.01, ***P < 0.001.

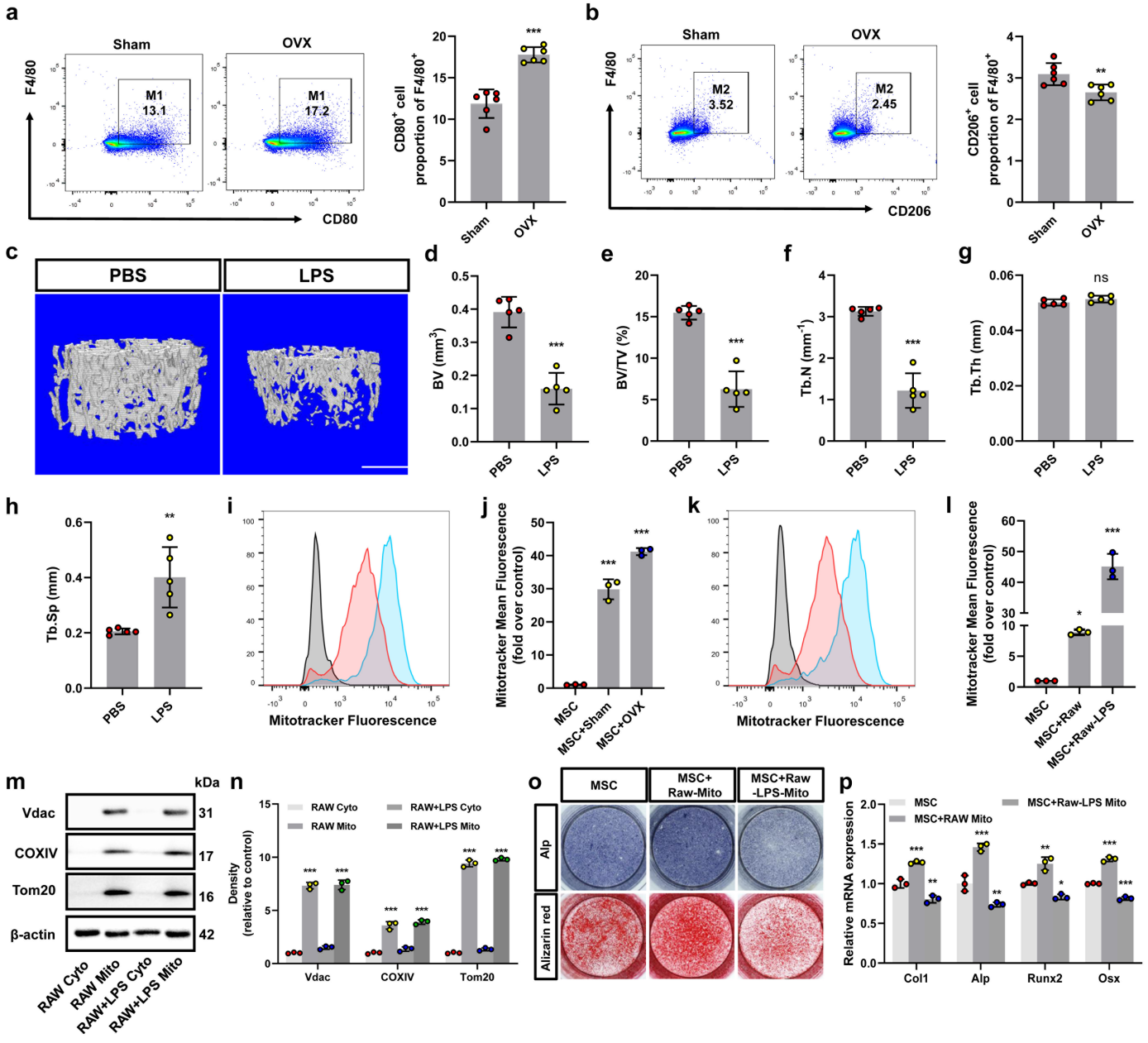

Figure 3

Mitochondrial dysfunction of macrophages affects the osteogenic differentiation of MSCs.

(a) Flow cytometry analysis (left) and quantification of CD80F4/80 macrophages in total bone marrow cells (right) (n = 6). (b) Flow cytometry analysis (left) and quantification of CD206F4/80 macrophages in total bone marrow cells (right) (n = 6). (c-h) Representative Micro-CT 3D structures of distal femurs of PBS and LPS-treated mice. Scale bar, 500 μm (c) and analysis of BV (d), BV/TV (e), Tb.N (f), Tb.Th (g) and Tb.Sp (h) (n = 6). (i, j) Flow cytometric analysis (i) and quantification of mean fluorescence intensity (j) of Mitotracker Deep Red-labeled mitochondrial internalization by MSCs in the presence of Sham (red line) or OVX-treated (blue line) macrophages. Grey line represents untreated MSCs (n = 3). (k,l) Flow cytometric analysis and quantification of MSCs incubated with untreated or LPS-treated macrophages, relative to untreated MSCs (n = 3). (m,n) Western blotting and quantification of mitochondrial proteins in isolated cytoplasm (Cyto) and mitochondria (Mito) from control and LPS-treated macrophages (n = 3). (o) Representative images of ALP and ARS staining in MSCs incubated with untreated Mito or LPS-treated Mito, and untreated MSCs (n = 3). (p) qPCR analysis of Col1, Alp, Runx2 and Osx expression under osteogenic conditions (n = 3). *P < 0.05, **P < 0.01, ***P < 0.001.

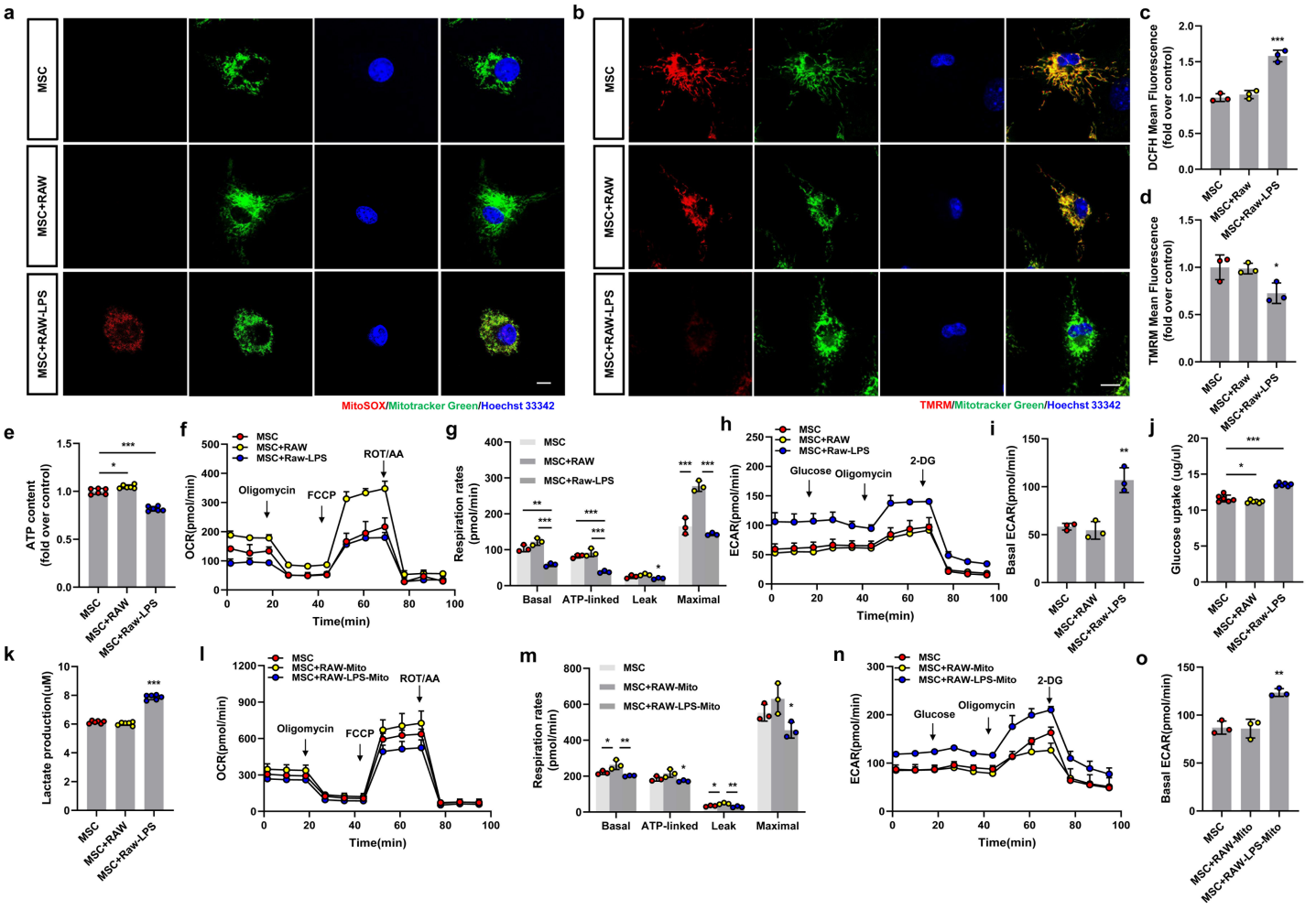

Figure 4

Macrophages and their derived mitochondria affect the metabolic status of MSCs.

(a, c) Mitochondrial ROS production was analyzed by MitoSOX and DCFH-DA staining. The mean fluorescence intensity was quantified as a measure of cellular reactive oxygen species production (n = 3). Scale bar, 5 μm. (b, d) Analysis by confocal microscopy and FACS to quantify MMPs. The intensity of TMRM staining reflected MMP (n = 3). Scale bar, 5 μm. (e) Relative ATP levels of MSCs incubated with untreated or LPS-treated macrophages compared with untreated MSCs (n = 6). (f, g) OCR (f), basal respiration, ATP-linked respiration, proton leak and maximal respiration (g) of the indicated cells (n = 3). (h, i) ECAR of indicated cells (n = 3). (j, k) Effects of glucose uptake (j) and lactate production (k) of MSCs cultured alone or in the presence of untreated or LPS-treated macrophages (n = 6). (l, m) OCR (l), basal respiration, ATP-linked respiration, proton leak and maximal respiration (m) of MSCs cultured alone or in the presence of untreated Mito or LPS-treated Mito (n = 3). (n, o) ECAR of MSCs cultured alone or in the presence of untreated Mito or LPS-treated Mito (n = 3). *P < 0.05, **P < 0.01, ***P < 0.001.

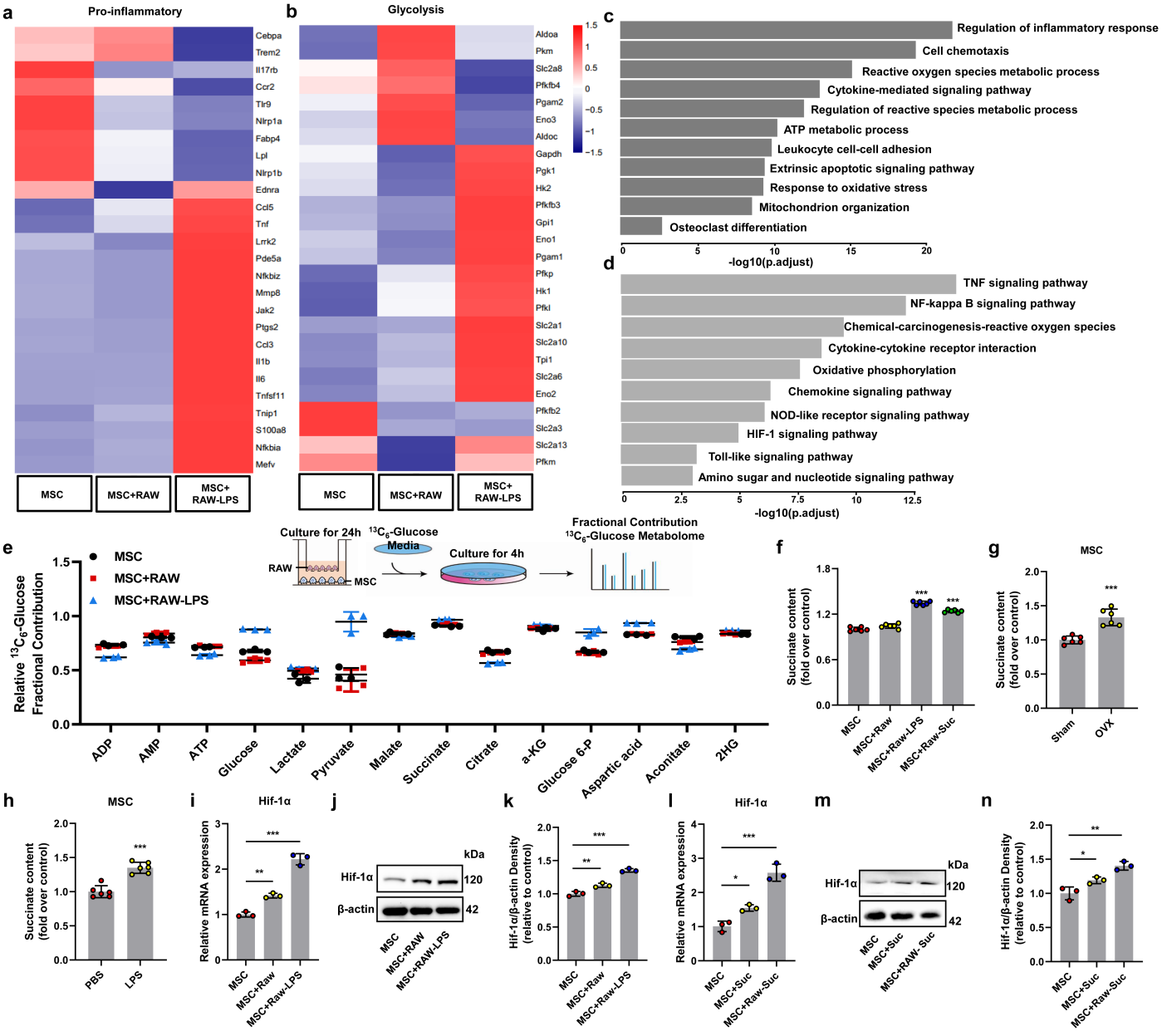

Figure 5

Mitochondrial transfer causes abnormal accumulation of succinate in MSCs.

(a–d) RNA-seq analysis of MSCs cultured alone or in the presence of untreated or LPS-treated macrophages. Pro-inflammatory genes (a), glycolysis genes (b), GO analysis (c), KEGG analysis (d) (n=3). (e) Partial contribution of $^{13}C_6$-glucose to the selection of relevant metabolites (n = 3). (f) Succinate content in MSCs cultured alone or in the presence of untreated or LPS-treated or succinate-treated macrophages (n = 3). (g, h) Succinate levels in MSCs (n = 6).

(i-k) qPCR analysis (i) and western blotting (j, k) to determine the levels of Hif-1α in MSCs incubated with untreated or LPS-treated macrophages compared to untreated MSCs (n = 3). (j, k) Western blot and quantitative determination of mitochondrial proteins and Hif-1α (n = 3). (l-n) qPCR analysis (l) and western blotting (m, n) to determine the levels of Hif-1α in MSCs incubated with untreated or succinate-treated macrophages compared to untreated MSCs (n = 3). *P < 0.05, **P < 0.01, ***P < 0.001.

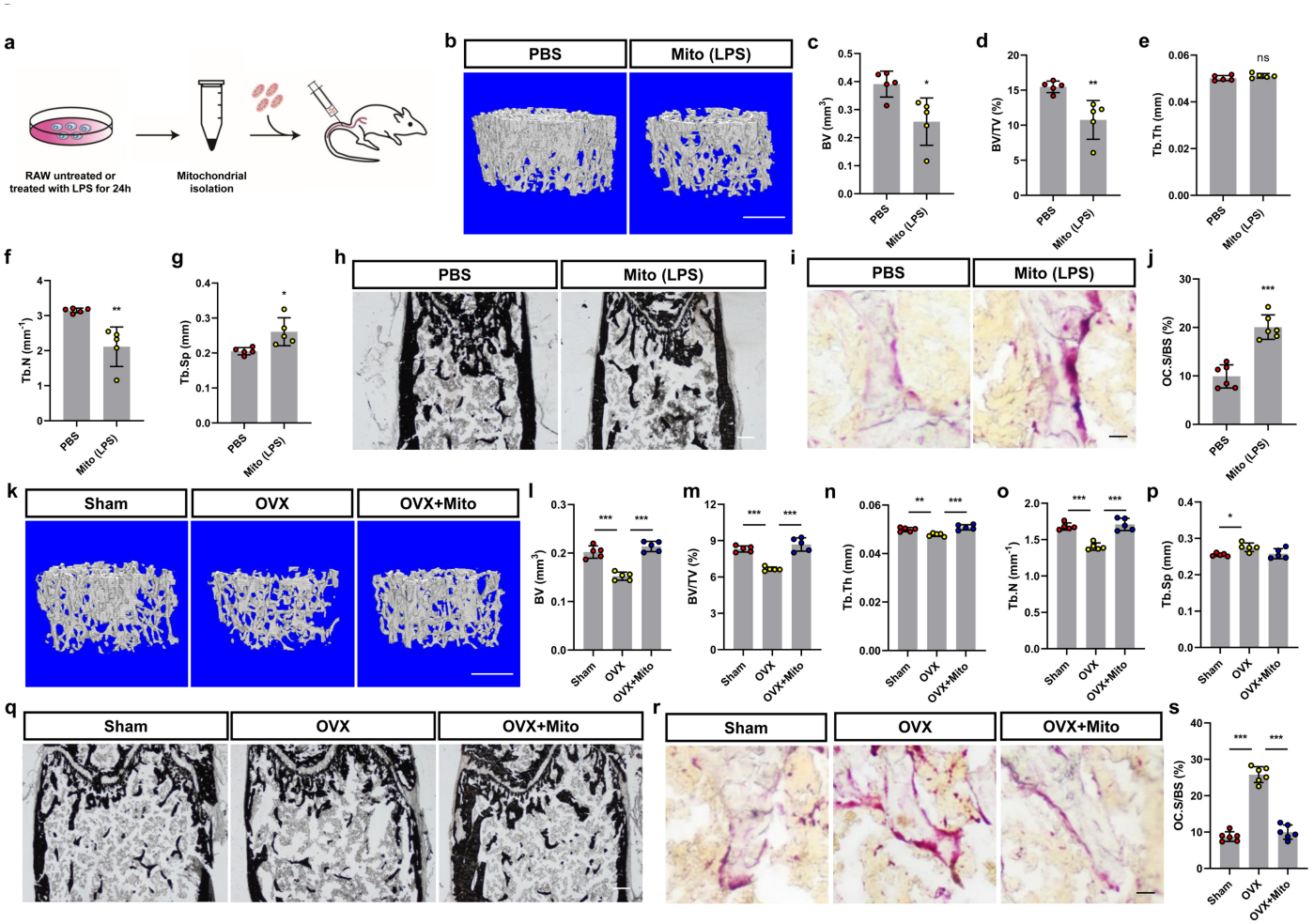

Figure 6

Mitochondrial transfer maintains bone health *in vivo*.

(a) Schematic showing mitochondrial application and treatment. (b-g) Mice received tail vein injections of LPS-treated Mito (100 μg dissolved in 100 μl PBS) or PBS twice a week for 3 weeks. Bone phenotypes were then analyzed (b). Scale bar, 500 μm. BV (c), BV/TV (d), Tb.N (e), Tb.Th (f) and Tb.Sp (g) analysis (n = 6). (h) Representative images of Von Kossa staining of distal femoral metaphysis from PBS and Mito (LPS) mice. Scale bar, 1000 μm (n = 3). (i, j) Representative images of representative TRAP staining of the distal femur in Sham, OVX and OVX + Mito mice (i). Scale bar, 100 μm. Quantification of the area of osteoclasts on the surface of trabecular bone (OC.S/BS) (j) (n = 6). (k–p) Representative Mico-CT images of femurs from Sham, OVX and OVX+Mito mice (k). Scale bar, 500 μm. (l-p) BV (l), BV/TV (m), Tb.N (n), Tb.Th (o) and Tb.Sp (p) analysis (n = 6). (q) Representative images of Von Kossa staining of distal femoral metaphysis from Sham, OVX and OVX+Mito mice. Scale bar, 1000 μm (n = 3). (r,s) Representative images of representative TRAP staining of the distal femur in Sham, OVX and OVX+Mito mice (r). Scale bar, 100 μm. The area of osteoclasts (OC.S/BS) on the surface of trabecular bone was quantified (s) (n = 6). *P < 0.05, **P < 0.01, ***P < 0.001.

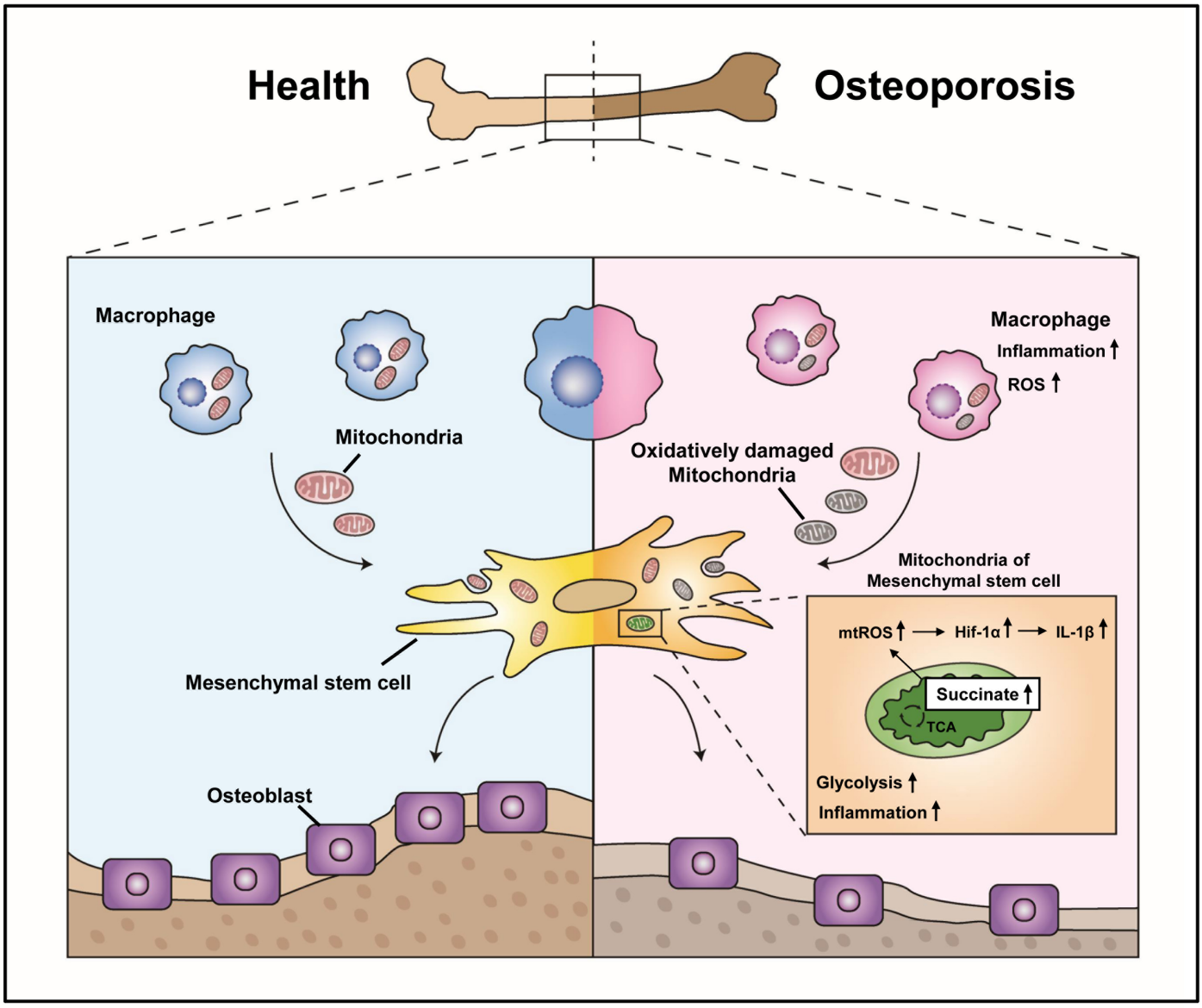

Figure 7

Schematic showing the mode of action of intercellular mitochondrial transfer of macrophages and MSCs in the bone environment to affect bone metabolism.

Our findings reveal that mitochondrial transfer may have emerged as a new mode of regulating cellular crosstalk in the bone environment. When macrophages are in an osteoporotic state, they release mitochondria with oxidative damage, triggering elevated ROS and mitochondrial dysfunction in MSCs. Metabolic dysfunction in MSCs leads to intracellular succinate accumulation, which promotes elevated levels of inflammation, which in turn affects osteogenic differentiation.

Supplementary Files

This is a list of supplementary files associated with this preprint. Click to download.

- SupplementaryTable.docx
- SupplementaryVideo1.mp4
- SupplementaryFigures.docx